Study of Dimuon Production in Photon-Photon Collisions and Measurement of QED Photon Structure Functions at LEP

DELPHI Collaboration

Abstract

Muon pair production in the process $e^+e^- \to e^+e^-\mu^+\mu^-$ is studied using the data taken at LEP1 ($\sqrt{s} \simeq m_Z$) with the DELPHI detector during the years 1992-1995. The corresponding integrated luminosity is 138.5 pb^{-1}. The QED predictions have been tested over the whole Q^2 range accessible at LEP1 (from several GeV$^2/c^4$ to several hundred GeV$^2/c^4$) by comparing experimental distributions with distributions resulting from Monte Carlo simulations using various generators. Selected events are used to extract the leptonic photon structure function F_2^γ. Azimuthal correlations are used to obtain information on additional structure functions, F_A^γ and F_B^γ, which originate from interference terms of the scattering amplitudes. The measured ratios F_A^γ/F_2^γ and F_B^γ/F_2^γ are significantly different from zero and consistent with QED predictions.

arXiv:hep-ex/0105084v1 28 May 2001

P.Abreu[22], W.Adam[52], T.Adye[38], P.Adzic[12], I.Ajinenko[44], Z.Albrecht[18], T.Alderweireld[2], G.D.Alekseev[17], R.Alemany[51], T.Allmendinger[18], P.P.Allport[23], S.Almehed[25], U.Amaldi[9,29], N.Amapane[47], S.Amato[49], E.G.Anassontzis[3], P.Andersson[46], A.Andreazza[9], S.Andringa[22], P.Antilogus[26], W-D.Apel[18], Y.Arnoud[9], B.Åsman[46], J-E.Augustin[26], A.Augustinus[9], P.Baillon[9], P.Bambade[20], F.Barao[22], G.Barbiellini[48], R.Barbier[26], D.Y.Bardin[17], G.Barker[18], A.Baroncelli[40], M.Battaglia[16], M.Baubillier[24], K-H.Becks[54], M.Begalli[6], A.Behrmann[54], P.Beilliere[8], Yu.Belokopytov[9], N.C.Benekos[33], A.C.Benvenuti[5], C.Berat[15], M.Berggren[24], D.Bertrand[2], M.Besancon[41], M.Bigi[47], M.S.Bilenky[17], M-A.Bizouard[20], D.Bloch[10], H.M.Blom[32], M.Bonesini[29], M.Boonekamp[41], P.S.L.Booth[23], A.W.Borgland[4], G.Borisov[20], C.Bosio[43], O.Botner[50], E.Boudinov[32], B.Bouquet[20], C.Bourdarios[20], T.J.V.Bowcock[23], I.Boyko[17], I.Bozovic[12], M.Bozzo[14], M.Bracko[45], P.Branchini[40], R.A.Brenner[50], P.Bruckman[9], J-M.Brunet[8], L.Bugge[34], T.Buran[34], B.Buschbeck[52], P.Buschmann[54], S.Cabrera[51], M.Caccia[28], M.Calvi[29], T.Camporesi[9], V.Canale[39], F.Carena[9], L.Carroll[23], C.Caso[14], M.V.Castillo Gimenez[51], A.Cattai[9], F.R.Cavallo[5], V.Chabaud[9], Ph.Charpentier[9], P.Checchia[37], G.A.Chelkov[17], R.Chierici[47], P.Chliapnikov[9,44], P.Chochula[7], V.Chorowicz[26], J.Chudoba[31], K.Cieslik[19], P.Collins[9], R.Contri[14], E.Cortina[51], G.Cosme[20], F.Cossutti[9], H.B.Crawley[1], D.Crennell[38], S.Crepe[15], G.Crosetti[14], J.Cuevas Maestro[35], S.Czellar[16], M.Davenport[9], W.Da Silva[24], G.Della Ricca[48], P.Delpierre[27], N.Demaria[9], A.De Angelis[48], W.De Boer[18], C.De Clercq[2], B.De Lotto[48], A.De Min[37], L.De Paula[49], H.Dijkstra[9], L.Di Ciaccio[9,39], J.Dolbeau[8], K.Doroba[53], M.Dracos[10], J.Drees[54], M.Dris[33], A.Duperrin[26], J-D.Durand[9], G.Eigen[4], T.Ekelof[50], G.Ekspong[46], M.Ellert[50], M.Elsing[9], J-P.Engel[10], M.Espirito Santo[22], G.Fanourakis[12], D.Fassouliotis[12], J.Fayot[24], M.Feindt[18], A.Fenyuk[44], A.Ferrer[51], E.Ferrer-Ribas[20], F.Ferro[14], S.Fichet[24], A.Firestone[1], U.Flagmeyer[54], H.Foeth[9], E.Fokitis[33], F.Fontanelli[14], B.Franek[38], A.G.Frodesen[4], R.Fruhwirth[52], F.Fulda-Quenzer[20], J.Fuster[51], A.Galloni[23], D.Gamba[47], S.Gamblin[20], M.Gandelman[49], C.Garcia[51], C.Gaspar[9], M.Gaspar[49], U.Gasparini[37], Ph.Gavillet[9], E.N.Gazis[33], D.Gele[10], N.Ghodbane[26], I.Gil[51], F.Glege[54], R.Gokieli[9,53], B.Golob[9,45], G.Gomez-Ceballos[42], P.Goncalves[22], I.Gonzalez Caballero[42], G.Gopal[38], L.Gorn[1], Yu.Gouz[44], V.Gracco[14], J.Grahl[1], E.Graziani[40], P.Gris[41], G.Grosdidier[20], K.Grzelak[53], J.Guy[38], C.Haag[18], F.Hahn[9], S.Hahn[54], S.Haider[9], A.Hallgren[50], K.Hamacher[54], J.Hansen[34], F.J.Harris[36], V.Hedberg[9,25], S.Heising[18], J.J.Hernandez[51], P.Herquet[2], H.Herr[9], T.L.Hessing[36], J.-M.Heuser[54], E.Higon[51], S-O.Holmgren[46], P.J.Holt[36], S.Hoorelbeke[2], M.Houlden[23], J.Hrubec[52], M.Huber[18], K.Huet[2], G.J.Hughes[23], K.Hultqvist[9,46], J.N.Jackson[23], R.Jacobsson[9], P.Jalocha[19], R.Janik[7], Ch.Jarlskog[25], G.Jarlskog[25], P.Jarry[41], B.Jean-Marie[20], D.Jeans[36], E.K.Johansson[46], P.Jonsson[26], C.Joram[9], P.Juillot[10], L.Jungermann[18], F.Kapusta[24], K.Karafasoulis[12], S.Katsanevas[26], E.C.Katsoufis[33], R.Keranen[18], G.Kernel[45], B.P.Kersevan[45], B.A.Khomenko[17], N.N.Khovanski[17], A.Kiiskinen[16], B.King[23], A.Kinvig[23], N.J.Kjaer[9], O.Klapp[54], H.Klein[9], P.Kluit[32], P.Kokkinias[12], V.Kostioukhine[44], C.Kourkoumelis[3], O.Kouznetsov[41], M.Krammer[52], E.Kriznic[45], Z.Krumstein[17], P.Kubinec[7], J.Kurowska[53], K.Kurvinen[16], J.W.Lamsa[1], D.W.Lane[1], V.Lapin[44], J-P.Laugier[41], R.Lauhakangas[16], G.Leder[52], F.Ledroit[15], V.Lefebure[2], L.Leinonen[46], A.Leisos[12], R.Leitner[31], J.Lemonne[2], G.Lenzen[54], V.Lepeltier[20], T.Lesiak[19], M.Lethuillier[41], J.Libby[36], W.Liebig[54], D.Liko[9], A.Lipniacka[9,46], I.Lippi[37], B.Loerstad[25], J.G.Loken[36], J.H.Lopes[49], J.M.Lopez[42], R.Lopez-Fernandez[15], D.Loukas[12], P.Lutz[41], L.Lyons[36], J.MacNaughton[52], J.R.Mahon[6], A.Maio[22], A.Malek[54], T.G.M.Malmgren[46], S.Maltezos[33], V.Malychev[17], F.Mandl[52], J.Marco[42], R.Marco[42], B.Marechal[49], M.Margoni[37], J-C.Marin[9], C.Mariotti[9], A.Markou[12], C.Martinez-Rivero[20], F.Martinez-Vidal[51], S.Marti i Garcia[9], J.Masik[13], N.Mastroyiannopoulos[12], F.Matorras[42], C.Matteuzzi[29], G.Matthiae[39], F.Mazzucato[37], M.Mazzucato[37], M.Mc Cubbin[23], R.Mc Kay[1], R.Mc Nulty[23], G.Mc Pherson[23], C.Meroni[28], W.T.Meyer[1], A.Miagkov[44], E.Migliore[9], L.Mirabito[26], W.A.Mitaroff[52], U.Mjoernmark[25], T.Moa[46], M.Moch[18], R.Moeller[30], K.Moenig[9,11], M.R.Monge[14], D.Moraes[49], X.Moreau[24], P.Morettini[14], G.Morton[36], U.Mueller[54], K.Muenich[54], M.Mulders[32], C.Mulet-Marquis[15], R.Muresan[25], W.J.Murray[38], B.Muryn[19], G.Myatt[36], T.Myklebust[34], F.Naraghi[15], M.Nassiakou[12], F.L.Navarria[5], S.Navas[51], K.Nawrocki[53], P.Negri[29], N.Neufeld[9], R.Nicolaidou[41], B.S.Nielsen[30], P.Niezurawski[53], M.Nikolenko[10,17], V.Nomokonov[16], A.Nygren[25], V.Obraztsov[44], A.G.Olshevski[17], A.Onofre[22], R.Orava[16], G.Orazi[10], K.Osterberg[16], A.Ouraou[41], M.Paganoni[29], S.Paiano[5], R.Pain[24], R.Paiva[22], J.Palacios[36], H.Palka[19], Th.D.Papadopoulou[9,33], K.Papageorgiou[12], L.Pape[9], C.Parkes[9], F.Parodi[14], U.Parzefall[23], A.Passeri[40], O.Passon[54], T.Pavel[25], M.Pegoraro[37], L.Peralta[22], M.Pernicka[52], A.Perrotta[5], C.Petridou[48], A.Petrolini[14], H.T.Phillips[38], F.Pierre[41], M.Pimenta[22], E.Piotto[28], T.Podobnik[45], M.E.Pol[6], G.Polok[19], P.Poropat[48], V.Pozdniakov[17], P.Privitera[39], N.Pukhaeva[17], A.Pullia[29], D.Radojicic[36], S.Ragazzi[29], H.Rahmani[33], J.Rames[13], P.N.Ratoff[21], A.L.Read[34], P.Rebecchi[9], N.G.Redaelli[28], M.Regler[52], J.Rehn[18], D.Reid[32], R.Reinhardt[54], P.B.Renton[36], L.K.Resvanis[3], F.Richard[20], J.Ridky[13], G.Rinaudo[47], I.Ripp-Baudot[10], O.Rohne[34], A.Romero[47], P.Ronchese[37], E.I.Rosenberg[1], P.Rosinsky[7], P.Roudeau[20], T.Rovelli[5], Ch.Royon[41], V.Ruhlmann-Kleider[41], A.Ruiz[42], H.Saarikko[16], Y.Sacquin[41], A.Sadovsky[17], G.Sajot[15], J.Salt[51], D.Sampsonidis[12], M.Sannino[14], Ph.Schwemling[24], B.Schwering[54], U.Schwickerath[18], F.Scuri[48], P.Seager[21], Y.Sedykh[17], A.M.Segar[36], N.Seibert[18], R.Sekulin[38], R.C.Shellard[6], M.Siebel[54], L.Simard[41], F.Simonetto[37], A.N.Sisakian[17], G.Smadja[26], N.Smirnov[44], O.Smirnova[25], G.R.Smith[38], A.Sopczak[18], R.Sosnowski[53], T.Spassov[22], E.Spiriti[40], S.Squarcia[14], C.Stanescu[40], S.Stanic[45], M.Stanitzki[18], K.Stevenson[36], A.Stocchi[20], J.Strauss[52], R.Strub[10], B.Stugu[4], M.Szczekowski[53], M.Szeptycka[53], T.Tabarelli[29], A.Taffard[23], O.Tchikilev[44], F.Tegenfeldt[50], F.Terranova[29], J.Thomas[36], J.Timmermans[32], N.Tinti[5], L.G.Tkatchev[17], M.Tobin[23], S.Todorova[10], A.Tomaradze[2], B.Tome[22], A.Tonazzo[9], L.Tortora[40], P.Tortosa[51], G.Transtromer[25], D.Treille[9], G.Tristram[8], M.Trochimczuk[53],

C.Troncon[28], M-L.Turluer[41], I.A.Tyapkin[17], S.Tzamarias[12], O.Ullaland[9], V.Uvarov[44], G.Valenti[9,5], E.Vallazza[48], C.Vander Velde[2], P.Van Dam[32], W.Van den Boeck[2], W.K.Van Doninck[2], J.Van Eldik[9,32], A.Van Lysebetten[2], N.van Remortel[2], I.Van Vulpen[32], G.Vegni[28], L.Ventura[37], W.Venus[38,9], F.Verbeure[2], P.Verdier[26], M.Verlato[37], L.S.Vertogradov[17], V.Verzi[39], D.Vilanova[41], L.Vitale[48], E.Vlasov[44], A.S.Vodopyanov[17], G.Voulgaris[3], V.Vrba[13], H.Wahlen[54], C.Walck[46], A.J.Washbrook[23], C.Weiser[9], D.Wicke[54], J.H.Wickens[2], G.R.Wilkinson[36], M.Winter[10], M.Witek[19], G.Wolf[9], J.Yi[1], O.Yushchenko[44], A.Zalewska[19], P.Zalewski[53], D.Zavrtanik[45], E.Zevgolatakos[12], N.I.Zimin[17,25], A.Zintchenko[17], Ph.Zoller[10], G.C.Zucchelli[46], G.Zumerle[37]

[1]Department of Physics and Astronomy, Iowa State University, Ames IA 50011-3160, USA
[2]Physics Department, Univ. Instelling Antwerpen, Universiteitsplein 1, B-2610 Antwerpen, Belgium
 and IIHE, ULB-VUB, Pleinlaan 2, B-1050 Brussels, Belgium
 and Faculté des Sciences, Univ. de l'Etat Mons, Av. Maistriau 19, B-7000 Mons, Belgium
[3]Physics Laboratory, University of Athens, Solonos Str. 104, GR-10680 Athens, Greece
[4]Department of Physics, University of Bergen, Allégaten 55, NO-5007 Bergen, Norway
[5]Dipartimento di Fisica, Università di Bologna and INFN, Via Irnerio 46, IT-40126 Bologna, Italy
[6]Centro Brasileiro de Pesquisas Físicas, rua Xavier Sigaud 150, BR-22290 Rio de Janeiro, Brazil
 and Depto. de Física, Pont. Univ. Católica, C.P. 38071 BR-22453 Rio de Janeiro, Brazil
 and Inst. de Física, Univ. Estadual do Rio de Janeiro, rua São Francisco Xavier 524, Rio de Janeiro, Brazil
[7]Comenius University, Faculty of Mathematics and Physics, Mlynska Dolina, SK-84215 Bratislava, Slovakia
[8]Collège de France, Lab. de Physique Corpusculaire, IN2P3-CNRS, FR-75231 Paris Cedex 05, France
[9]CERN, CH-1211 Geneva 23, Switzerland
[10]Institut de Recherches Subatomiques, IN2P3 - CNRS/ULP - BP20, FR-67037 Strasbourg Cedex, France
[11]Now at DESY-Zeuthen, Platanenallee 6, D-15735 Zeuthen, Germany
[12]Institute of Nuclear Physics, N.C.S.R. Demokritos, P.O. Box 60228, GR-15310 Athens, Greece
[13]FZU, Inst. of Phys. of the C.A.S. High Energy Physics Division, Na Slovance 2, CZ-180 40, Praha 8, Czech Republic
[14]Dipartimento di Fisica, Università di Genova and INFN, Via Dodecaneso 33, IT-16146 Genova, Italy
[15]Institut des Sciences Nucléaires, IN2P3-CNRS, Université de Grenoble 1, FR-38026 Grenoble Cedex, France
[16]Helsinki Institute of Physics, HIP, P.O. Box 9, FI-00014 Helsinki, Finland
[17]Joint Institute for Nuclear Research, Dubna, Head Post Office, P.O. Box 79, RU-101 000 Moscow, Russian Federation
[18]Institut für Experimentelle Kernphysik, Universität Karlsruhe, Postfach 6980, DE-76128 Karlsruhe, Germany
[19]Institute of Nuclear Physics and University of Mining and Metalurgy, Ul. Kawiory 26a, PL-30055 Krakow, Poland
[20]Université de Paris-Sud, Lab. de l'Accélérateur Linéaire, IN2P3-CNRS, Bât. 200, FR-91405 Orsay Cedex, France
[21]School of Physics and Chemistry, University of Lancaster, Lancaster LA1 4YB, UK
[22]LIP, IST, FCUL - Av. Elias Garcia, 14-1°, PT-1000 Lisboa Codex, Portugal
[23]Department of Physics, University of Liverpool, P.O. Box 147, Liverpool L69 3BX, UK
[24]LPNHE, IN2P3-CNRS, Univ. Paris VI et VII, Tour 33 (RdC), 4 place Jussieu, FR-75252 Paris Cedex 05, France
[25]Department of Physics, University of Lund, Sölvegatan 14, SE-223 63 Lund, Sweden
[26]Université Claude Bernard de Lyon, IPNL, IN2P3-CNRS, FR-69622 Villeurbanne Cedex, France
[27]Univ. d'Aix - Marseille II - CPP, IN2P3-CNRS, FR-13288 Marseille Cedex 09, France
[28]Dipartimento di Fisica, Università di Milano and INFN, Via Celoria 16, IT-20133 Milan, Italy
[29]Università degli Studi di Milano - Bicocca, Via Emanuelli 15, IT-20126 Milan, Italy
[30]Niels Bohr Institute, Blegdamsvej 17, DK-2100 Copenhagen Ø, Denmark
[31]IPNP of MFF, Charles Univ., Areal MFF, V Holesovickach 2, CZ-180 00, Praha 8, Czech Republic
[32]NIKHEF, Postbus 41882, NL-1009 DB Amsterdam, The Netherlands
[33]National Technical University, Physics Department, Zografou Campus, GR-15773 Athens, Greece
[34]Physics Department, University of Oslo, Blindern, NO-1000 Oslo 3, Norway
[35]Dpto. Fisica, Univ. Oviedo, Avda. Calvo Sotelo s/n, ES-33007 Oviedo, Spain
[36]Department of Physics, University of Oxford, Keble Road, Oxford OX1 3RH, UK
[37]Dipartimento di Fisica, Università di Padova and INFN, Via Marzolo 8, IT-35131 Padua, Italy
[38]Rutherford Appleton Laboratory, Chilton, Didcot OX11 OQX, UK
[39]Dipartimento di Fisica, Università di Roma II and INFN, Tor Vergata, IT-00173 Rome, Italy
[40]Dipartimento di Fisica, Università di Roma III and INFN, Via della Vasca Navale 84, IT-00146 Rome, Italy
[41]DAPNIA/Service de Physique des Particules, CEA-Saclay, FR-91191 Gif-sur-Yvette Cedex, France
[42]Instituto de Fisica de Cantabria (CSIC-UC), Avda. los Castros s/n, ES-39006 Santander, Spain
[43]Dipartimento di Fisica, Università degli Studi di Roma La Sapienza, Piazzale Aldo Moro 2, IT-00185 Rome, Italy
[44]Inst. for High Energy Physics, Serpukov P.O. Box 35, Protvino, (Moscow Region), Russian Federation
[45]J. Stefan Institute, Jamova 39, SI-1000 Ljubljana, Slovenia and Laboratory for Astroparticle Physics,
 Nova Gorica Polytechnic, Kostanjeviska 16a, SI-5000 Nova Gorica, Slovenia,
 and Department of Physics, University of Ljubljana, SI-1000 Ljubljana, Slovenia
[46]Fysikum, Stockholm University, Box 6730, SE-113 85 Stockholm, Sweden
[47]Dipartimento di Fisica Sperimentale, Università di Torino and INFN, Via P. Giuria 1, IT-10125 Turin, Italy
[48]Dipartimento di Fisica, Università di Trieste and INFN, Via A. Valerio 2, IT-34127 Trieste, Italy
 and Istituto di Fisica, Università di Udine, IT-33100 Udine, Italy
[49]Univ. Federal do Rio de Janeiro, C.P. 68528 Cidade Univ., Ilha do Fundão BR-21945-970 Rio de Janeiro, Brazil
[50]Department of Radiation Sciences, University of Uppsala, P.O. Box 535, SE-751 21 Uppsala, Sweden
[51]IFIC, Valencia-CSIC, and D.F.A.M.N., U. de Valencia, Avda. Dr. Moliner 50, ES-46100 Burjassot (Valencia), Spain
[52]Institut für Hochenergiephysik, Österr. Akad. d. Wissensch., Nikolsdorfergasse 18, AT-1050 Vienna, Austria
[53]Inst. Nuclear Studies and University of Warsaw, Ul. Hoza 69, PL-00681 Warsaw, Poland
[54]Fachbereich Physik, University of Wuppertal, Postfach 100 127, DE-42097 Wuppertal, Germany

1   Introduction

The study of the process $e^+e^- \rightarrow e^+e^-\mu^+\mu^-$ provides a good way to test QED up to the fourth order of α. The photon structure can be studied by measuring photon structure functions which can be extracted in the so-called "single tagged" mode (Fig. 1), where one of the scattered electrons[1] is detected ("tagged") in an electromagnetic calorimeter while the other scattered electron goes undetected ("untagged"). This process can also be used as a reference one for studies of the hadronic structure function of the photon, providing a basis for a better understanding of the detector performance and for checking the analysis procedure.

Previous measurements of muon pair production in both the single tagged mode and the double tagged mode (where the scattered electron and positron are both detected) have shown good agreement with QED predictions [1,2,3,4,5,6,7,8,9,10,11,12,13,14], with one exception [9] where an excess of data events was observed in the double tag mode.

This study, based on the data collected by the DELPHI collaboration at LEP1 at centre-of-mass energies from 89.4 to 93 GeV, complements those results. It improves on previous DELPHI measurements of the leptonic photon structure function F_2^γ [11] by including all the LEP1 statistics and increasing the Q^2 coverage by an order of magnitude. This paper also presents results of studies of the azimuthal correlations, which are used to extract the ratios of the structure functions F_A^γ/F_2^γ and F_B^γ/F_2^γ.

2   Event kinematics

In the single tagged mode, where the tagged and untagged electrons are scattered with polar angles θ_{tag} and θ_{untag} and energies E_{tag} and E_{untag} respectively, and the probe and target photons have four-momenta $q = (x_{tag}E_{beam}, \vec{q})$ and $p = (x_{untag}E_{beam}, \vec{p})$, the cross section of the reaction $e^+e^- \rightarrow e^+e^- X$ is given by [15]:

$$\frac{d^3\sigma}{dxdQ^2dx_{untag}} = \frac{dn(x_{untag})}{dx_{untag}} \times \frac{d^2\sigma(e\gamma \rightarrow eX)}{dxdQ^2}. \tag{1}$$

These two factors, the flux of target photons and the $e\gamma$ cross section respectively, are given by:

$$\frac{dn(x_{untag})}{dx_{untag}} = \frac{\alpha}{\pi x_{untag}} \left\{ \left(1 + (1 - x_{untag})^2\right) \ln\left(\frac{2E_{beam}(1 - x_{untag})}{m_e x_{untag}} \sin\frac{\theta_{untag}^{max}}{2}\right) - 1 + x_{untag} \right\}, \tag{2}$$

$$\frac{d^2\sigma(e\gamma \rightarrow eX)}{dxdQ^2} = \frac{2\pi\alpha^2}{xQ^4} \left\{ \left(1 + (1-y)^2\right) F_2^\gamma(x, Q^2, P^2) - y^2 F_L^\gamma(x, Q^2, P^2) \right\}. \tag{3}$$

Here F_2^γ and F_L^γ are structure functions of the photon, α is the QED coupling constant, $Q^2 = -q^2 \simeq 4E_{tag}E_{beam}\sin^2(\theta_{tag}/2)$ is the squared 4-momentum transfer, $P^2 = -p^2$ is the virtuality of the target photon, and x and y are the Bjorken variables

$$x = \frac{Q^2}{2q \cdot p} = \frac{Q^2}{W_{\gamma\gamma}^2 + Q^2 + P^2}, \qquad y = \frac{p \cdot q}{p \cdot k} \simeq \frac{Q^2}{sxx_{untag}} = 1 - \frac{E_{tag}}{E_{beam}} \cos^2\frac{\theta_{tag}}{2} \tag{4}$$

where $W_{\gamma\gamma}^2 = (q + p)^2$ is the invariant mass of the $\gamma\gamma$ (or $\mu^+\mu^-$) system, k is the initial four-vector of the tagged electron, and $s = 4E_{beam}^2$.

---
[1]Throughout the paper the term "electron" will be used for the tagged electron/positron

The structure function F_2^γ can be extracted from the dependence of the cross section on x and Q^2. But F_L^γ is small and is weighted by the small factor y^2, making its direct measurement impractical.

However, additional structure functions can be studied by looking at azimuthal correlations of the final state particles. The differential cross section of the process can be written as [16]

$$\frac{d^4\sigma(e\gamma \to e\mu^+\mu^-)}{dxdyd\cos\theta^*d\chi/4\pi} = \frac{2\pi\alpha^2}{Q^2} \cdot \frac{1 + (1-y)^2}{xy} \times$$
$$\left\{ (2x\tilde{F}_T + \epsilon(y)\tilde{F}_L) - \rho(y)\tilde{F}_A \cos\chi + \frac{1}{2}\epsilon(y)\tilde{F}_B \cos 2\chi \right\}, \quad (5)$$

where χ is the azimuthal angle, defined in the $\gamma\gamma^*$ centre-of-mass frame as the angle between the planes formed by the photon axis and the muon and the scattered electron respectively (Fig. 2), and θ^* is the angle between the muon and the photon axis. The functions $\rho(y)$ and $\epsilon(y)$ are given by $\rho(y) = (2-y)\sqrt{1-y}/(1+(1-y)^2)$ and $\epsilon(y) = 2(1-y)/(1+(1-y)^2)$ [17] and can be taken equal to 1 in the accessible kinematical region. The differential structure functions $\tilde{F}_T$, $\tilde{F}_L$, $\tilde{F}_A$, and $\tilde{F}_B$ give the corresponding standard structure functions F_T, F_L, F_A, and F_B after integrating appropriately over $\cos\theta^*$ (see section 7.2) taking into account that F_A is antisymmetric in $\cos\theta^*$ [18]. The cross section can then be written as

$$\frac{d^3\sigma(e\gamma \to e\mu^+\mu^-)}{dxdyd\chi/2\pi} \simeq \frac{2\pi\alpha^2}{Q^2} \cdot \frac{1 + (1-y)^2}{xy} \times$$
$$F_2^\gamma \left(1 - (F_A^\gamma/F_2^\gamma)\cos\chi + \frac{1}{2}(F_B^\gamma/F_2^\gamma)\cos 2\chi \right). \quad (6)$$

The structure functions F_i^γ are combinations of transition amplitudes for the different helicity states of the photons. The structure function F_B^γ is related to the interference term between the two transverse helicity states of the photons. It is identical to F_L^γ, which is related to the longitudinal polarization of the virtual photon, in leading order and for massless muons.

3 DELPHI detector

The DELPHI detector has been described in detail elsewhere [19,20]. In this analysis, the scattered electron was tagged using

- the Small Angle Tagger (SAT), the main luminosity monitor during 1991-93, covering polar angles from 2.5° to 8° (172° to 177.5°); it was made of alternating layers of lead sheets (0.9 mm thick) and plastic scintillator fibres (1 mm in diameter), aligned parallel to the beam;
- the Small angle TIle Calorimeter (STIC), the main luminosity monitor since 1994, covering polar angles from 1.7° to 10.3° (169.7° to 178.3°); the STIC is a sampling calorimeter with 49 sandwiches of 3.4 mm steel-laminated lead plates and 3 mm thick scintillator tiles giving a total thickness of $\sim$27 radiation lengths;
- the Forward ElectroMagnetic Calorimeter (FEMC) covering from 10° to 36.5° (143.5° to 170°) in polar angle, consisting of two 5 m diameter disks containing a total of 9064 lead glass blocks.

The energy resolution of the tagging calorimeters was around 5% in SAT and FEMC and 3% in STIC for an incident electron energy of 45 GeV.

For muon identification, DELPHI contained barrel and forward muon detectors, each consisting of at least 4 layers of drift chambers. The muon chambers covered 78% of the solid angle.

Combining the information from the tracking detectors, the relative momentum resolution σ_p/p varied from $0.001 \times p$ to $0.01 \times p$ (p in GeV/c), depending on the polar angle of the charged particle.

4 Monte Carlo simulation

Two event generators were used in order to simulate the signal process $e^+e^- \to e^+e^-\mu^+\mu^-$: BDKRC [21] which includes only the multiperipheral diagram (Fig.1) together with QED radiative corrections, and DIAG36 [22] which lacks the QED radiative corrections but includes also the bremsstrahlung, annihilation and conversion diagrams. DIAG36 was used to check the role of these additional diagrams.

Several generators were used to estimate the backgrounds to the process studied: BDKRC [21] was used to simulate $e^+e^- \to e^+e^-\tau^+\tau^-$, TWOGAM [23] to simulate hadron production in two-photon collisions, DYMU3 [24] for the $e^+e^- \to \mu^+\mu^-(\gamma)$ process, and KORALZ [25] for $e^+e^- \to \tau^+\tau^-(\gamma)$.

The generated events were passed through the full simulation of the DELPHI detector and reconstructed using the same program as for the data.

5 Event selection and correction

Events were selected as single tagged dimuon candidates if the following requirements were met.

- There was a cluster in one of the electromagnetic calorimeters with an energy deposition greater than $0.6 \times E_{beam}$ (hereafter called the tagged electron). If the cluster lay within the polar angle range 20° - 160°, it was linked to a detected charged particle.
- There were exactly two additional particles with opposite charges and polar angles between 20° and 160°. The relative errors on their momenta were less than 1. Their impact parameters with respect to the average interaction point were below 4 cm in the transverse plane and 10 cm along the beam. Their track lengths seen in the tracking detectors were at least 30 cm. Their momenta were above 0.5 GeV/c and 2.5 GeV/c and the sum of their momenta was below 30 GeV/c.
- At least one of the additional particles with a momentum greater than 2.5 GeV/c was identified as a muon by the DELPHI standard muon tagging algorithm [20].
- The invariant mass of the two additional particles was above 1.7 GeV/c^2. This requirement reduced the contribution from diagrams other than the multiperipheral one to below 0.25% for the low Q^2 and 2% for the high Q^2 sample according to the DIAG36 generator, and avoided possible problems with the soft part of the spectrum due to trigger or muon tagging inefficiency.
- Finally, double-tagged events were rejected by requiring there to be no energy deposit exceeding $0.3 \times E_{beam}$ in the detector arm (defined as $\theta = 0° - 90°$ and $\theta = 90° - 180°$) opposite that containing the tagged electron.

Using the high redundancy of the trigger [20], the trigger inefficiency was found to be negligible for these events.

In order to improve the measurements of the tagged electron parameters (energy and angles), the following procedures were used.

1. To avoid edge effects, the tagged electron was required to lie in the polar angle range $3° < \theta < 7.6°$ ($172.4° < \theta < 177°$) for the SAT, $2.5° < \theta < 9°$ ($171° < \theta < 177.5°$) for the STIC, or $11° < \theta < 35°$ ($145° < \theta < 169°$) for the FEMC.

2. To improve the θ measurements in the SAT, which had a limited granularity, the radial position of the cluster was corrected using the function found from the comparison of the experimental radial distribution for Bhabha events with the theoretical one based on a $1/\theta^3$ cross section dependence (Fig. 3). This improved the Q^2 resolution from 6.0% to 2.9%.

3. To improve the θ measurements in the SAT and STIC, their alignments were checked using Bhabha event samples. The detector on the electron side had a mask in front of it to better define the acceptance at low θ. From the number of Bhabha events as a function of the electron azimuthal angle ϕ_1, it was possible to find the displacement of the mask relative to the beam line. The alignment on the opposite side was checked by looking at the difference of the measured polar angles $\theta_{tag} - \theta_{untag}$ of the scattered electron and positron as a function of the positron azimuthal angle ϕ_2 (Fig. 4). The dependencies observed were used to correct the measured polar angles. The errors of the fitted parameters were taken as uncertainties of the procedure, contributing 0.5% uncertainty on low values of Q^2.

4. A more accurate value of the tagged electron energy E_{tag} was calculated from the requirements of energy and longitudinal momentum conservation in the event:

$$E_{tag} = \frac{P_{\mu\mu} \cos\theta_{\mu\mu} + (2E_{beam} - E_{\mu\mu}) \cos\theta_{untag}}{\cos\theta_{untag} - \cos\theta_{tag}}, \tag{7}$$

where $P_{\mu\mu}$, $E_{\mu\mu}$ and $\theta_{\mu\mu}$ are the momentum, energy and polar angle of the muon system, and θ_{untag} is the polar angle of the untagged electron, assumed to be 0 or π. The improvement due to this method can be seen in Fig. 5, obtained from simulation, where the difference between the reconstructed and true (generated) tag energy $E_{tag} - E_{tag}^{gen}$ is shown as a function of the tag angle θ_{tag} using both the direct measurement of E_{tag} and this method.

6 Background

The following sources of background to the $\mu^+\mu^-$ event samples were considered:

- $e^+e^- \rightarrow e^+e^-\tau^+\tau^-$ with a τ decay product identified as a muon. The background from this process was found to be $(1.2\pm0.2)\%$ for the SAT and STIC tagged samples and $(5.7\pm1.1)\%$ for the FEMC, where the errors quoted are statistical.
- $e^+e^- \rightarrow \tau^+\tau^-(\gamma)$ with a hard radiated photon or a τ decay product faking a tagged electron. This background was found to be negligible for the SAT and STIC samples, and $(8.9\pm1.9)\%$ for the FEMC, after taking into account the on-peak versus off-peak luminosity distribution of the data.
- $e^+e^- \rightarrow \mu^+\mu^-(\gamma)$ with the radiated photon faking a tagged electron. This was found to be negligible due to the 30 GeV cut on the sum of the muon momenta.
- $e^+e^- \rightarrow e^+e^-\pi^+\pi^-$ with a pion misidentified as a muon. The ratio of the cross sections for pion pair and muon pair production in two-photon interactions falls to (1-5)% if the invariant mass of the produced pair is above 2.0 GeV/c^2 [26]. With the muon identification criteria described above, the probability to misidentify a pion

as a muon was below 1.5% (depending on the pion momentum), so this background was also negligible for all samples.

- other $e^+e^- \to e^+e^- + hadrons$ processes. These were also found to be negligible for all event samples.

- untagged $e^+e^- \to e^+e^-\mu^+\mu^-$ in coincidence with an off-momentum electron faking a tagged electron. The off-momentum electrons are beam electrons that have scattered off residual gas molecules inside the beam pipe. Using a method similar to the one described in [27], this background was estimated from $Z^0 \to \mu\mu$ events in coincidence with a similar off-momentum electron, multiplying by the ratio of the dimuon production cross sections from untagged two-photon interactions and from Z^0 decays, and was also found to be negligible.

7 Results

The numbers of selected data events after background subtraction are compared with the predictions of the signal Monte Carlo simulations in Table 1. The Q^2 ranges shown are calculated given the angular coverage of the detectors and the cut on the tag energy, and the average values $<Q^2>$ are taken from the data. Figs. 6 – 8 present the distributions of a standard set of observables for events tagged by the SAT, STIC and FEMC respectively.

Tagging detector	SAT	STIC	FEMC
Q^2 range (GeV^2/c^4)	$3.4-36.6$	$2.4-51.2$	$45.9-752.8$
$<Q^2>^{*)}$ (GeV^2/c^4)	13.0	12.1	120.0$^{**)}$
data	1357 ± 37	2875 ± 54	239 ± 18
BDKRC simulation	1362 ± 14	2884 ± 22	250 ± 6
DIAG36 simulation	1298 ± 25	2785 ± 55	236 ± 13

$^{*)}$ After requiring $E_{tag} > 0.75 \times E_{beam}$ (see text)
$^{**)}$ For events with $\theta_{tag} < 25°$ ($\theta_{tag} > 155°$) (see text)

Table 1: Numbers of selected events after background subtraction.

Table 1 and Figs. 6 - 8 show that the BDKRC and DIAG36 generators produce similar kinematical distributions, but DIAG36 gives somewhat lower numbers of selected events. In the kinematical region under study, the contribution of the additional diagrams in DIAG36 was found to be very small (see section 5). This difference (if real) should therefore be attributed to the effect of radiative corrections. The BDKRC generator was therefore used for the structure function studies below.

7.1 Extraction of F_2^γ

To extract F_2^γ, the experimental x distribution was divided by the Monte Carlo distribution weighted by the factor $\alpha/F_2^\gamma(x, Q^2)$, where $F_2^\gamma(x, Q^2)$ can be obtained from a simulated event sample using either a generator producing events according to a given F_2 or the photon flux approach described, for example, in [13] and briefly outlined below.

It follows from Eqs. (1-3) that, neglecting the small contribution from y^2 terms:

$$F_2^\gamma(x, Q^2, P^2) = \frac{d^2\sigma}{dxdQ^2}/\mathcal{W}(x, Q^2), \tag{8}$$

where the weight $\mathcal{W}(x, Q^2)$ is given by

$$\mathcal{W}(x, Q^2) = \frac{4\pi\alpha^2}{xQ^4} \int\limits_{x_{untag}^{min}}^{x_{untag}^{max}} \frac{dn(x_{untag})}{dx_{untag}} (1-y) \ dx_{untag}. \qquad (9)$$

To calculate the integration limits, the fractional energy of the target photon is extracted from the expressions for x and $W_{\gamma\gamma}$:

$$x_{untag} = \frac{2Q^2/sx - 2Q^2/s + \cos\Theta + \cos\theta_{untag} - x_{tag}(1+\cos\Theta)}{\cos\Theta + \cos\theta_{untag} + x_{tag}(1-\cos\Theta)}, \qquad (10)$$

where

$$\cos\Theta = \sin\theta_{tag}\sin\theta_{untag}\cos(\Delta\phi) - \cos\theta_{tag}\cos\theta_{untag}, \qquad (11)$$

and $\Delta\phi$ is the azimuthal angle between the scattered e^+ and e^-. In the single tag approximation, $\theta_{untag} \simeq 0$ so that (10) becomes:

$$x_{untag} = \frac{2Q^2/sx - 2Q^2/s - \cos\theta_{tag} + 1 - x_{tag}(1-\cos\theta_{tag})}{-\cos\theta_{tag} + 1 + x_{tag}(1+\cos\theta_{tag})}. \qquad (12)$$

The maximum and minimum x_{untag} values correspond to the minimum and maximum x_{tag} values, and these result from the tagging conditions:

$$x_{tag}^{max} = \min\left\{1 - \frac{E_{tag}^{min}}{E_{beam}}, 1 - \frac{Q^2}{s\sin^2(\theta_{tag}^{max}/2)}\right\}, \qquad x_{tag}^{min} = \max\left\{\frac{W_{\gamma\gamma}^2}{s}, 1 - \frac{Q^2}{s\sin^2(\theta_{tag}^{min}/2)}\right\} \qquad (13)$$

where E_{tag}^{min} is the lower cut on the tag energy and $\theta_{tag}^{min}(\theta_{tag}^{max})$ is the lower (upper) angular acceptance of the tagging device. E_{tag}^{min} was increased from $0.6 \times E_{beam}$ to $0.75 \times E_{beam}$ in order to keep the y^2 contribution small.

Fig. 9 shows the $F_2^\gamma(x)$ values obtained by both methods for a simulated event sample with STIC tagging conditions, demonstrating that they give similar results.

A fit to the QED prediction [15,28]

$$F_2^\gamma = \frac{\alpha}{\pi}x\left\{\left(x^2 + (1-x)^2\right)\ln\frac{W_{\gamma\gamma}^2}{m_\mu^2 + P^2x(1-x)} - 1 + 8x(1-x) - \frac{P^2x(1-x)}{m_\mu^2 + P^2x(1-x)}\right\}, \qquad (14)$$

where terms of order m_μ^2/Q^2 are neglected gives values of the effective average target photon virtuality P^2 of 0.022 ± 0.007 and 0.026 ± 0.006 GeV^2 for the first and second methods respectively, the errors quoted being statistical. For the SAT tagged events the first method, which was chosen for the further analysis, gives $P^2=0.032\pm0.007$ GeV^2, demonstrating the need to take the target photon virtuality into account in studies of F_2^γ.

The extracted structure function $< F_2^\gamma(x, Q^2) >$, transformed to $F_2^\gamma(x, < Q^2 >)$ using the ratio $F_2^\gamma(x, < Q^2 >)/ < F_2^\gamma(x, Q^2) >$ predicted by QED, is shown in Table 2 and Fig. 10, which present the weighted combination of the SAT and STIC results with $< Q^2 >= 12.5$ GeV^2/c^4 and the FEMC result with $< Q^2 >= 120$ GeV^2/c^4. The FEMC sample included only events with θ_{tag} below 25° (above 155°) in order to exclude the region with large background contamination (Fig. 8b), and the contribution from diagrams other than the multiperipheral one predicted by the BDKRC generator was subtracted. The structure function values have been corrected to the centres of the x bins by multiplying the measured average values of F_2^γ for each x bin by the ratio of the value of F_2^γ in the centre of the bin to the its average value over the bin predicted by QED. Systematic

errors due to the resolutions in Q^2 and x have been evaluated in simulation by varying these variables according to their resolutions and checking the effect on F_2^γ. The role of the observed discrepancy between the data and simulation in some θ_{tag} intervals (Fig. 3) was checked by weighting the contributions of events in those intervals according to their θ_{tag} values when producing the x distribution. The largest contribution to the systematic error comes from the Q^2 resolution.

Fits to the QED prediction (14) give $P^2 = 0.025 \pm 0.005$ and 0.073 ± 0.056 GeV^2 for the samples with low and high Q^2 respectively, in good agreement with the Monte Carlo prediction.

x	<0.1	0.1-0.2	0.2-0.3	0.3-0.4	0.4-0.5	0.5-0.6	0.6-0.7	0.7-0.8	>0.8
F_2^γ/α	0.106	0.273	0.426	0.515	0.573	0.645	0.743	0.942	1.152
stat. error	±0.008	±0.012	±0.017	±0.021	±0.024	±0.029	±0.038	±0.060	±0.112
syst. error	±0.023	±0.012	±0.012	±0.012	±0.004	±0.003	±0.021	±0.053	±0.094

x	<0.2	0.2-0.4	0.4-0.6	0.6-0.8	>0.8
F_2^γ/α	0.387	0.464	0.673	0.984	1.508
stat. error	±0.214	±0.133	±0.138	±0.162	±0.231
syst. error	±0.015	±0.051	±0.049	±0.026	±0.044

Table 2: The measured structure function F_2^γ for $<Q^2> = 12.5$ (upper table) and 120 GeV$^2/c^4$ (lower table).

7.2 Azimuthal correlations

In order to increase the observed azimuthal correlations of the final state particles, only events with $20° < \theta^* < 160°$ have been considered. Taking into account the anti-symmetry of F_A^γ in $\cos\theta^*$, events with $\cos\theta^* <0$ and $\cos\theta^* >0$ have been combined using the transformation $\chi \to \pi - \chi$.

The selected samples have been corrected for detector acceptance and efficiency using either bin-by-bin corrections over a two-dimensional grid of χ and θ^*, or a three-dimensional unfolding [29] in the space of the variables χ, θ^* and x. The corrected distributions (Fig. 11) were fitted to the expression:

$$dN/d\chi = C\left(1 + P_1 \cos\chi + P_2 \cos 2\chi\right) \tag{15}$$

where P_1 and P_2 are closely related to F_A^γ/F_2^γ and F_B^γ/F_2^γ, c.f. Eq. (6). The combined results were obtained by refitting the weighted sums of corrected distributions for the SAT and STIC samples (Fig. 12). The parameters determined from the fit are shown in Table 3.

The systematic effects were estimated using simulated events, varying the variables Q^2, $W_{\gamma\gamma}$, x, θ^* and χ according to their resolution, and adding the resulting variations of the fitted parameters in quadrature. This gave errors on the fitted parameters of about 0.02. The difference between the results obtained with the two different correction methods gave an additional systematic error of $0.02-0.06$.

The results obtained were extrapolated to the full θ^* and $W_{\gamma\gamma}$ ranges using the theoretical correction factors C_{P_1} and C_{P_2} shown in Table 3, which were obtained as ratios of the QED predicted structure functions [18] calculated for event samples generated in the

Q^2 range of 2.4-51.2 GeV^2 without and with the selection cuts. The results thus obtained for F_A^γ/F_2^γ and $\frac{1}{2}F_B^\gamma/F_2^\gamma$ are shown in Table 3 and Fig. 13. They are in agreement with the theoretical predictions [18] and with the results of other LEP experiments [13,14] (note the factor -1/2 difference of F_A^γ with [13] due to its different definition).

8 Conclusions

Muon pair production in single-tagged $\gamma\gamma$ collisions has been studied at $\sqrt{s} \simeq 91$ GeV using data collected by the DELPHI detector at LEP during the years 1992-95. Distributions of different event variables for Q^2 ranging from $\sim$2.5 to $\sim$750 GeV$^2/c^4$ are well reproduced by a Monte Carlo simulation based on QED.

The leptonic structure function F_2^γ has been measured for two regions of momentum transfer with average Q^2 values of 12.5 and 120 GeV$^2/c^4$.

Azimuthal correlations of final state particles have also been studied, giving information on additional structure functions F_A^γ and F_B^γ. The measured ratios F_A^γ/F_2^γ and F_B^γ/F_2^γ are significantly different from zero and consistent with QED expectations.

Acknowledgements

References

[1] H.J. Behrend et al. (CELLO Collab.), Phys. Lett. **B126** (1983) 384.

[2] M.P. Cain et al. (TPC/2γ Collab.), Phys. Lett. **B147** (1984) 232.

[3] Ch. Berger et al. (PLUTO Collab.), Z. Phys. **C27** (1985) 249.

[4] W. Bartel et al. (JADE Collab.), Z. Phys. **C30** (1986) 545.

[5] B. Adeva et al. (MARK J coolab.), Phys. Rev. **D38** (1988) 2665.

[6] H.J. Behrend et al. (CELLO Collab.), Z. Phys. **C43** (1989) 1.

[7] M. Petradza et al. (MARK II Collab.), Phys. Rev. **D42** (1990) 2171.

[8] M. Petradza et al. (HRS Collab.), Phys. Rev. **D42** (1990) 2180.

[9] Y.H. Ho et al. (AMY Collab.), Phys. Lett. **B244** (1990) 573.

[10] R. Akers et al. (OPAL Collab.), Z. Phys. **C60** (1993) 593.

[11] R. Abreu et al. (DELPHI Collab.), Z. Phys. **C69** (1996) 223.

[12] K. Ackerstaff et al. (OPAL Collab.), Z. Phys. **C74** (1997) 49.

[13] M. Acciarri et al. (L3 Collab.), Phys. Lett. **B438** (1998) 363.

[14] G. Abbiendi et al. (OPAL Collab.), Eur. Phys. J. **C11** (1999) 409.

[15] V.M. Budnev et al., Phys. Rep. **15** (1974) 181.

[16] P. Aurenche et al., 'Physics at LEP2', eds. G. Altarelli, T. Sjöstrand and F. Zwirner, CERN 96-01 (1996) Vol.1 p.291.

[17] C. Peterson, P.M. Zerwas and T.F. Walsh, Nucl. Phys. **B229** (1983) 301.

[18] S. Ong and P. Kessler, Mod. Phys. Lett. **A2** (1987) 683.
Note that in the expression for the helicity terms $I_{++,++} + I_{++,--}$ a factor β^2 is missing in front of $(1-u^2)$ and in the expression for $I_{++,00}$ there should be the first degree power in the denominator.

[19] P. Aarnio et al. (DELPHI Collab.), Nucl. Inst. Meth. **A303** (1991) 233.

[20] P. Abreu et al. (DELPHI Collab.), Nucl. Inst. Meth. **A378** (1996) 57.

[21] F.A. Berends, P.H. Daverveldt, R. Kleiss, Comp. Phys. Comm. **40** (1986) 271.

[22] F.A. Berends, P.H. Daverveldt, R. Kleiss, Comp. Phys. Comm. **40** (1986) 285.

[23] S. Nova, A. Olshevski and T. Todorov, 'Physics at LEP2', CERN 96-01 (1996) Vol.2 p.224; updated version described in 'Reports of the Working Groups on Precision Calculations for LEP2 Physics', CERN 2000-009 (2000) 243.

[24] J.E. Campagne and R. Zitoun, Z. Phys. **C43** (1989) 469.

[25] S. Jadach et al., Comp. Phys. Comm. **79** (1994) 503.

[26] Ch. Berger et al. (PLUTO Collab.), Phys. Lett. **B137** (1984) 267.

[27] P. Abreu et al. (DELPHI Collab.), Phys. Lett. **B342** (1995) 402.

[28] C. Berger and W. Wagner, Phys. Rep. **146** (1987) 1.

[29] G. D'Agostini, Nucl. Inst. Meth. **A362** (1995) 487.

x-interval	P_1			C_{P_1}
	SAT	STIC	Combined	
$x < 0.2$	$0.19 \pm 0.14 \pm 0.03$	$0.28 \pm 0.08 \pm 0.04$	0.25 ± 0.08	0.541
$0.2 < x < 0.4$	$0.22 \pm 0.09 \pm 0.03$	$0.20 \pm 0.06 \pm 0.02$	0.20 ± 0.05	0.701
$0.4 < x < 0.6$	$0.13 \pm 0.09 \pm 0.05$	$0.02 \pm 0.07 \pm 0.05$	0.06 ± 0.07	0.625
$x > 0.6$	$-0.41 \pm 0.10 \pm 0.07$	$-0.26 \pm 0.07 \pm 0.05$	-0.31 ± 0.07	0.849
all x	$-0.03 \pm 0.05 \pm 0.03$	$-0.03 \pm 0.03 \pm 0.03$	-0.03 ± 0.04	0.605

x-interval	P_2			C_{P_2}
	SAT	STIC	Combined	
$x < 0.2$	$0.06 \pm 0.12 \pm 0.03$	$-0.01 \pm 0.08 \pm 0.03$	0.01 ± 0.07	0.391
$0.2 < x < 0.4$	$0.13 \pm 0.08 \pm 0.03$	$0.16 \pm 0.06 \pm 0.02$	0.15 ± 0.05	0.512
$0.4 < x < 0.6$	$0.15 \pm 0.08 \pm 0.04$	$0.19 \pm 0.06 \pm 0.03$	0.17 ± 0.06	0.581
$x > 0.6$	$0.20 \pm 0.09 \pm 0.06$	$0.30 \pm 0.06 \pm 0.04$	0.27 ± 0.06	0.673
all x	$0.13 \pm 0.05 \pm 0.02$	$0.15 \pm 0.03 \pm 0.02$	0.15 ± 0.03	0.570

x-interval	F_A^γ/F_2^γ	$\frac{1}{2}F_B^\gamma/F_2^\gamma$
$x < 0.2$	0.135 ± 0.043	0.004 ± 0.027
$0.2 < x < 0.4$	0.140 ± 0.035	0.077 ± 0.026
$0.4 < x < 0.6$	0.038 ± 0.044	0.099 ± 0.035
$x > 0.6$	-0.263 ± 0.059	0.182 ± 0.040
all x	-0.018 ± 0.024	0.086 ± 0.017

Table 3: Parameters P_1 and P_2 of the fit to the azimuthal angle distributions for the SAT-tagged, STIC-tagged, and combined event samples with $Q^2 = 2.4 - 51.2$ GeV^2. The first error is statistical and the second is systematic. C_{P_1} and C_{P_2} are the correction factors to extrapolate the parameters to the full θ^* range (see text). The values extracted for F_A^γ/F_2^γ and $\frac{1}{2}F_B^\gamma/F_2^\gamma$ are shown with statistical and systematic errors added in quadrature.
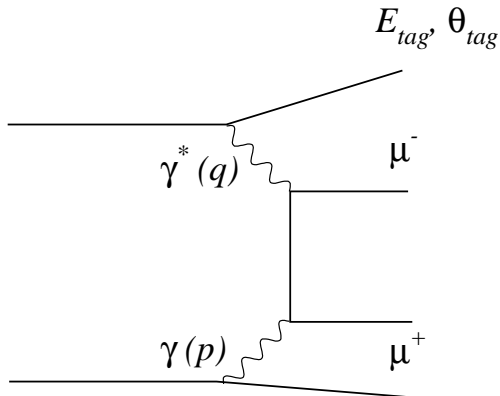
Figure 1: The dominant multiperipheral diagram for the reaction $e^+e^- \rightarrow e^+e^-\mu^+\mu^-$. E_{tag} and θ_{tag} are the energy and scattering angle of the tagged electron or positron.
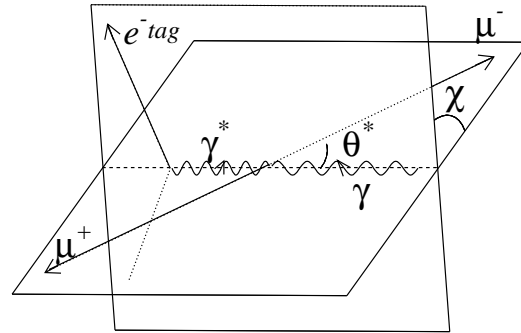
Figure 2: Definitions of the angles χ and θ^* in the $\gamma\gamma^*$ centre-of-mass system.
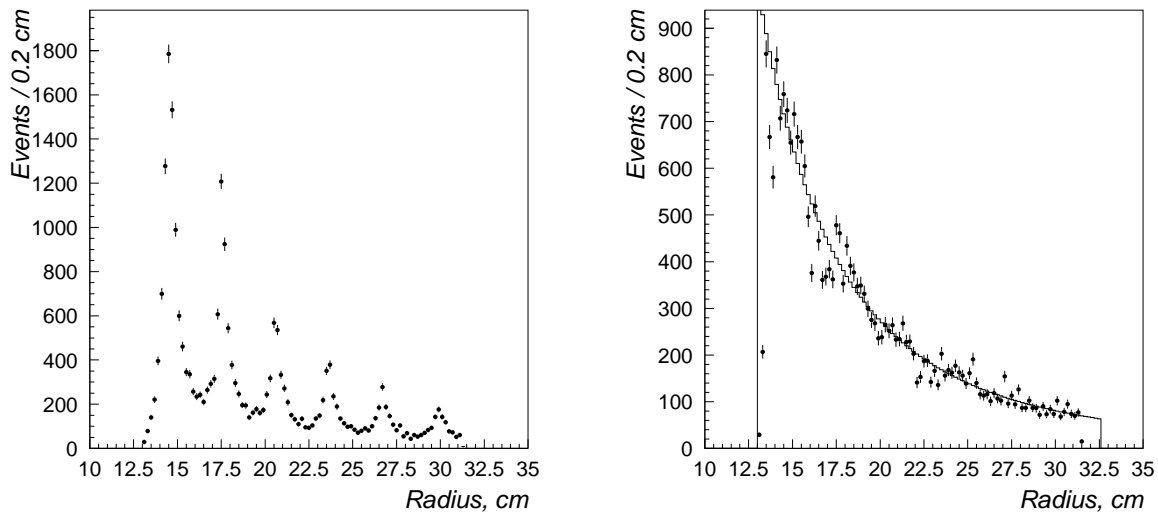
DELPHI

Figure 3: Distributions of the radial positions of Bhabha electrons in the SAT: left - before correcting the radial cluster positions, right - after correction. The line shows the result of the fit to the theoretical prediction.

DELPHI
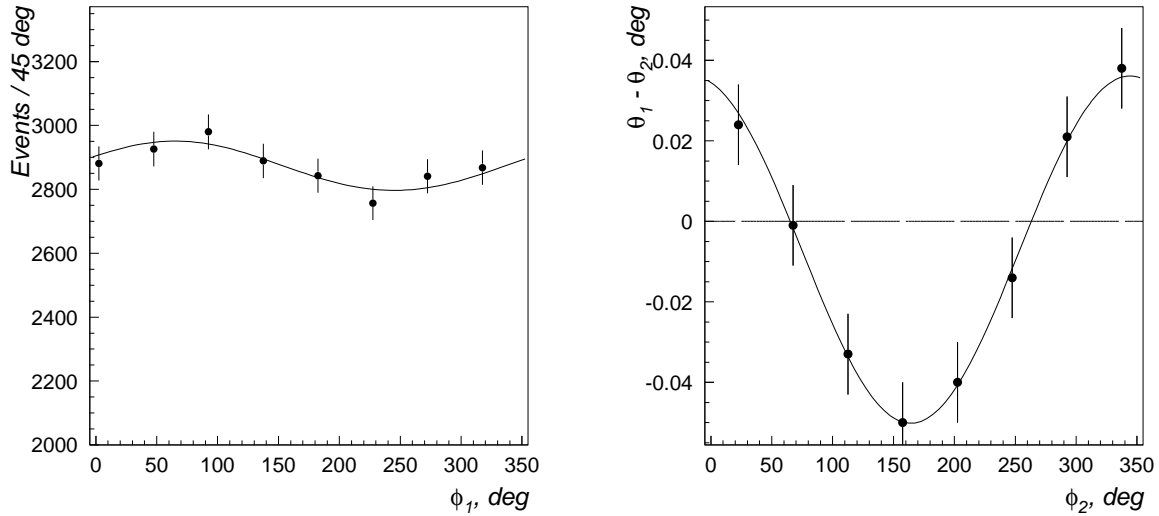
Figure 4: Left - number of detected Bhabha events as a function of the azimuthal angle for the SAT module with the mask. Right - difference of the polar angles of Bhabha electrons measured by the SAT modules as a function of the azimuthal angle. The lines show the results of the fits.

DELPHI
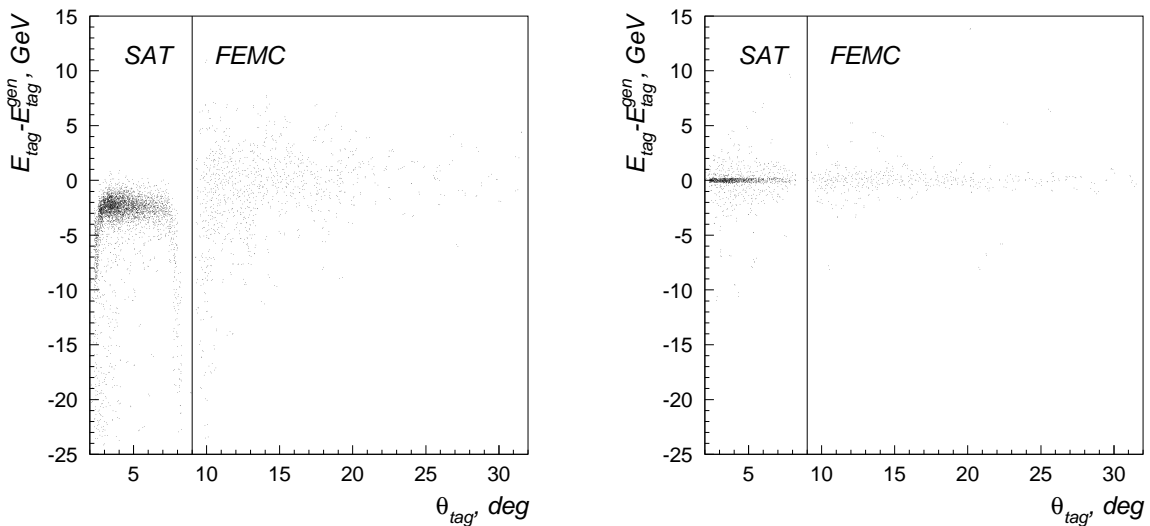
Figure 5: Difference of reconstructed and true (generated) tag energy E_{tag} versus the tag angle θ_{tag} in simulated events: left - measured value of E_{tag}, right - E_{tag} value calculated from the kinematics of the event.

DELPHI
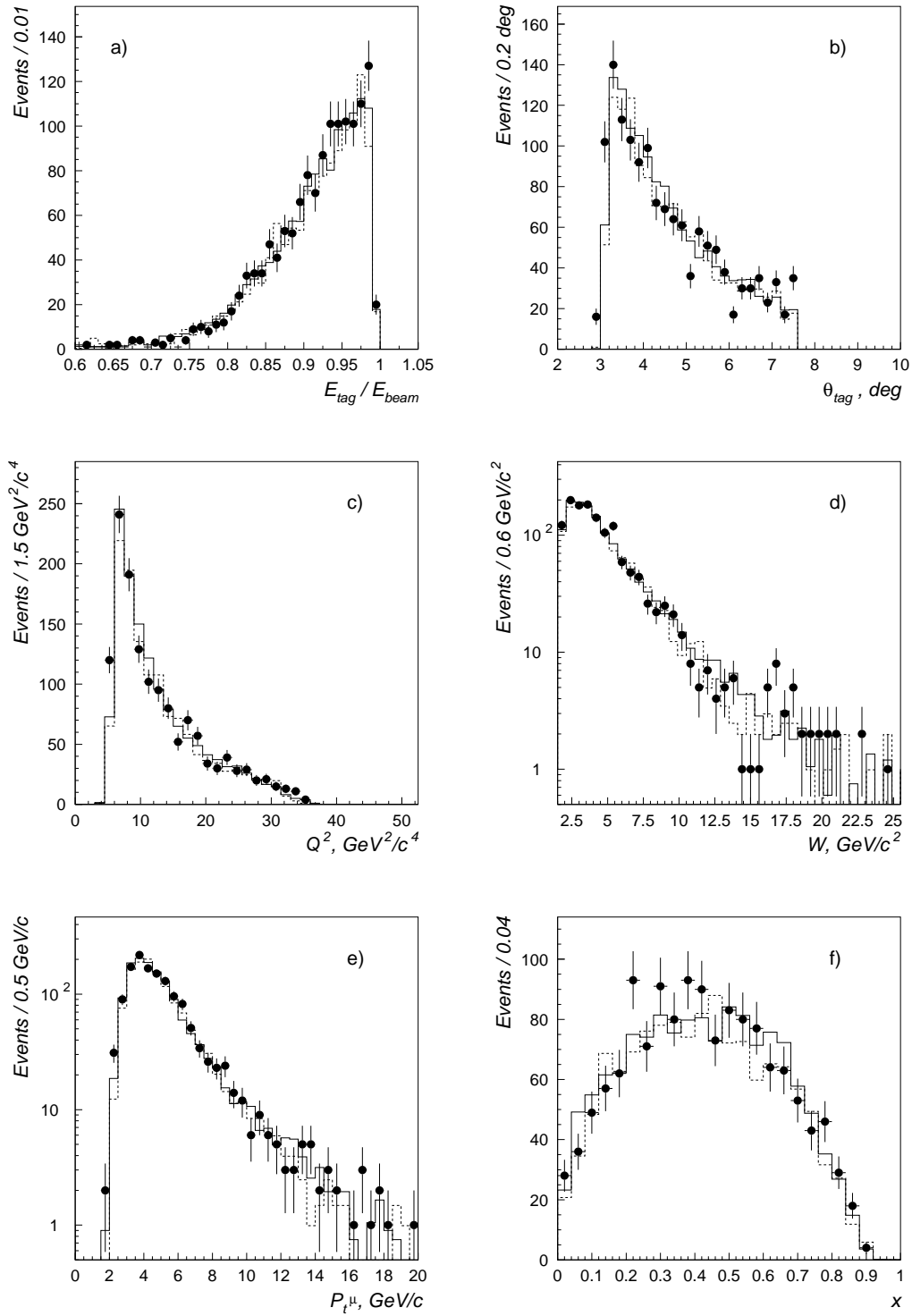
Figure 6: Distributions for the SAT single tagged events: a) E_{tag}/E_{beam}, b) θ_{tag} ($180° - \theta_{tag}$ for positrons), c) squared momentum transfer Q^2, d) invariant mass of muon pair, e) sum of the transverse momenta of the muons, f) value of x. The points correspond to the background subtracted data, the solid line to the BDKRC simulation, and the dashed line to the DIAG36 simulation.

DELPHI
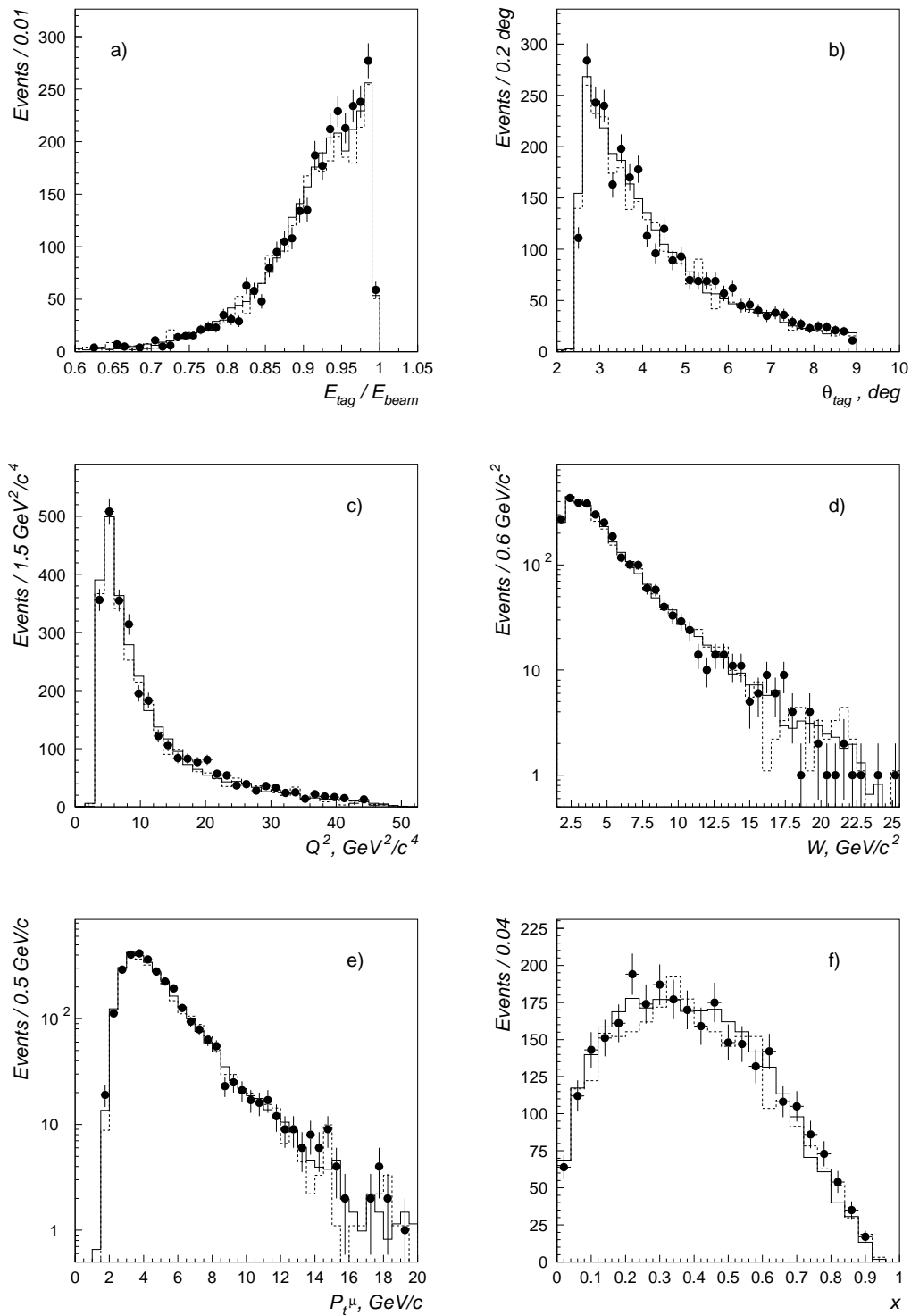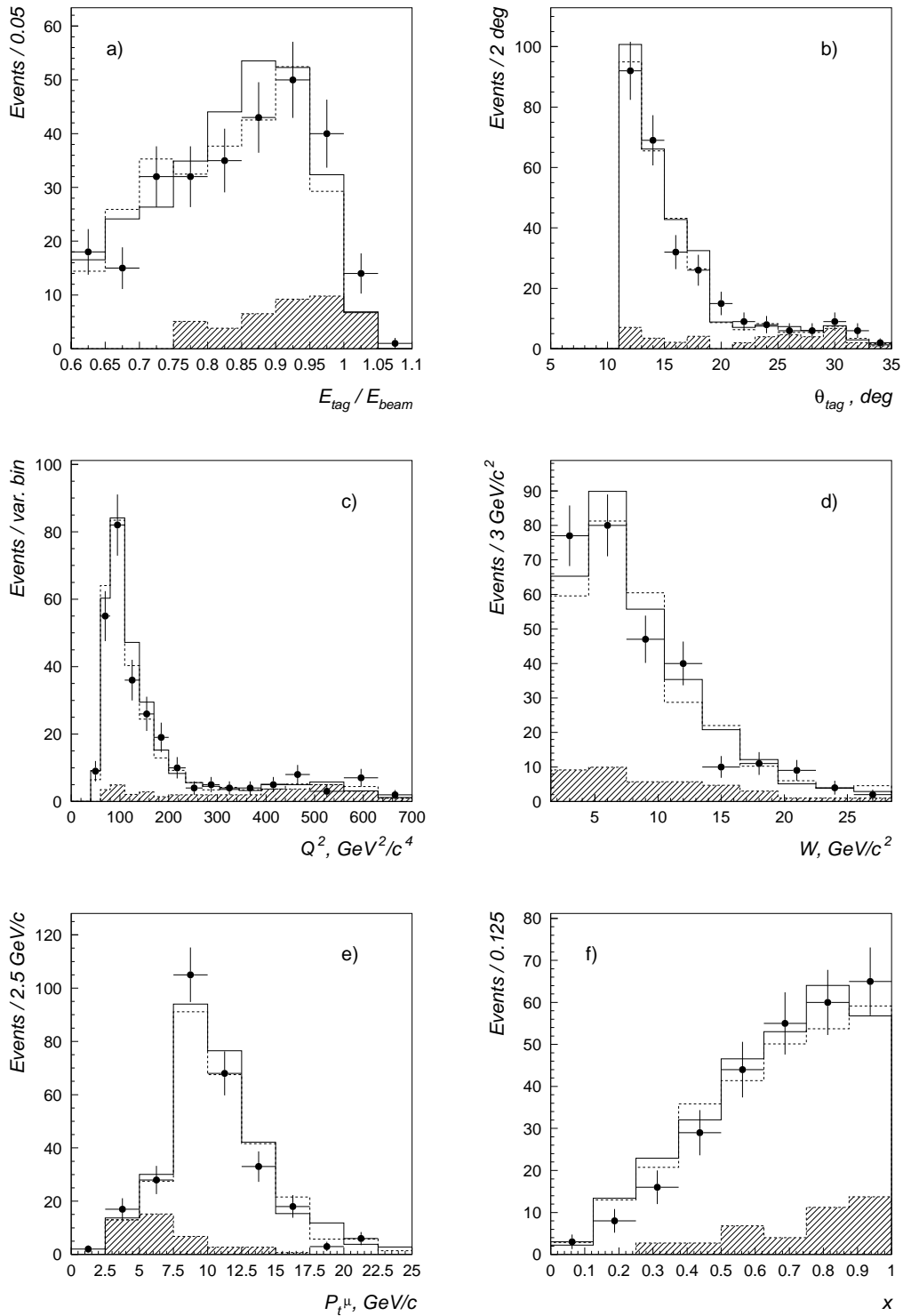

Figure 7: The same as Fig. 6 for the STIC single tagged events.

DELPHI

Figure 8: The same as Figs. 6 and 7 for the FEMC single tagged events except that the background, relatively much larger here than in Figs. 6 and 7 and shown here by the hatched histograms, has in this case been added to the simulated distributions rather than subtracted from the data.

DELPHI
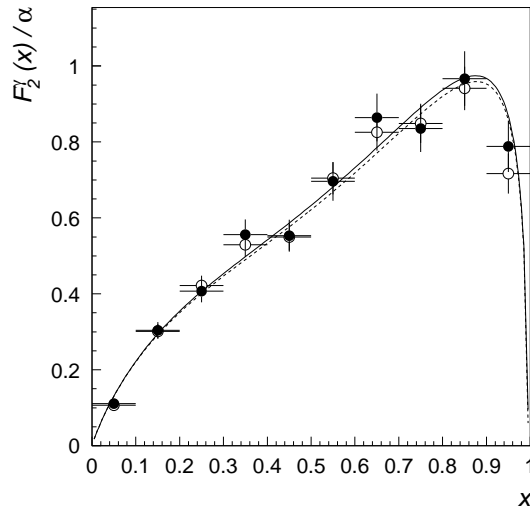
Figure 9: $F_2^\gamma(x)$ for $< Q^2 >= 12.5$ GeV$^2/c^4$ extracted from a simulated STIC tagged event sample (points) and the fit to the QED expression (lines): full circles and solid lines are for the extraction using the simulation with known F_2, open circles and dashed lines for the extraction using the photon flux approach.

DELPHI
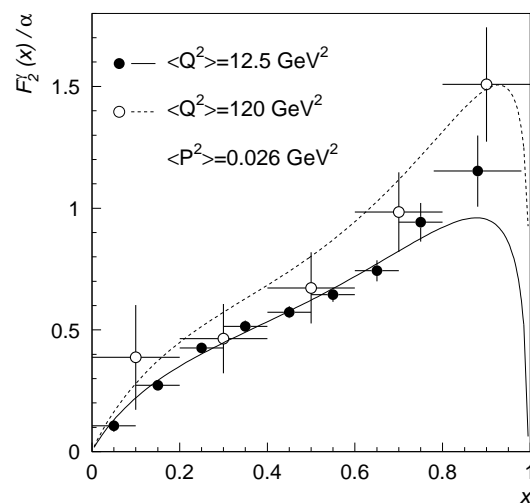
Figure 10: $F_2^\gamma(x)$ extracted from the combined SAT and STIC data ($< Q^2 >= 12.5$ GeV$^2/c^4$, full circles), and from the FEMC data ($< Q^2 >= 120$ GeV$^2/c^4$, open circles). Statistical and systematic errors are added in quadrature. The solid and dashed lines show the QED predictions with $P^2=0.026$ GeV$^2/c^4$ for the low Q^2 and high Q^2 samples, respectively.

DELPHI
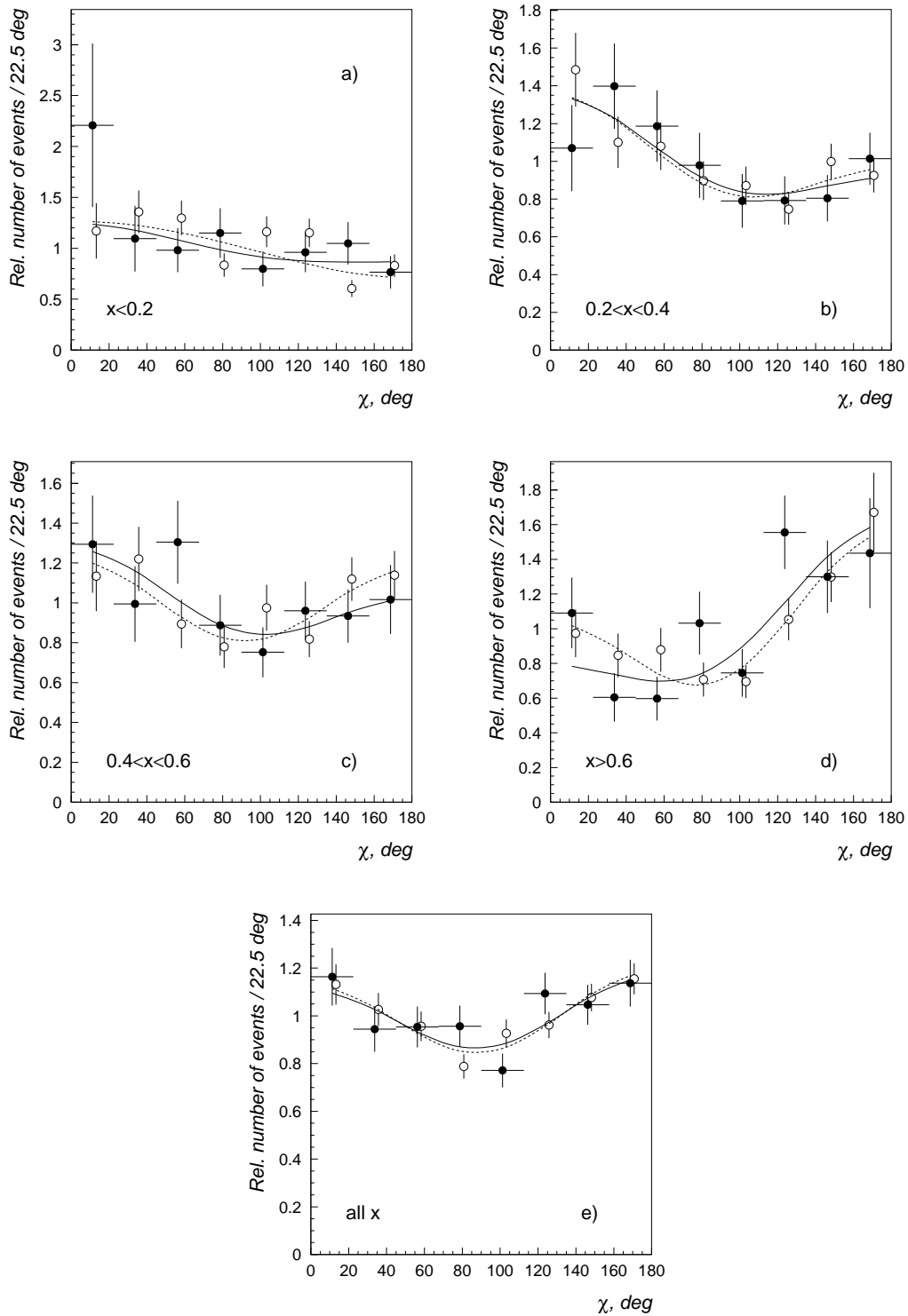

Figure 11: Azimuthal angle distributions corrected for detector inefficiency: a) $x <0.2$, b) $0.2< x <0.4$, c) $0.4< x <0.6$, d) $x >0.6$, e) all x. The lines correspond to the results of the fit. Full circles and solid line are for the SAT single tagged events, open circles and dashed line for the STIC events.
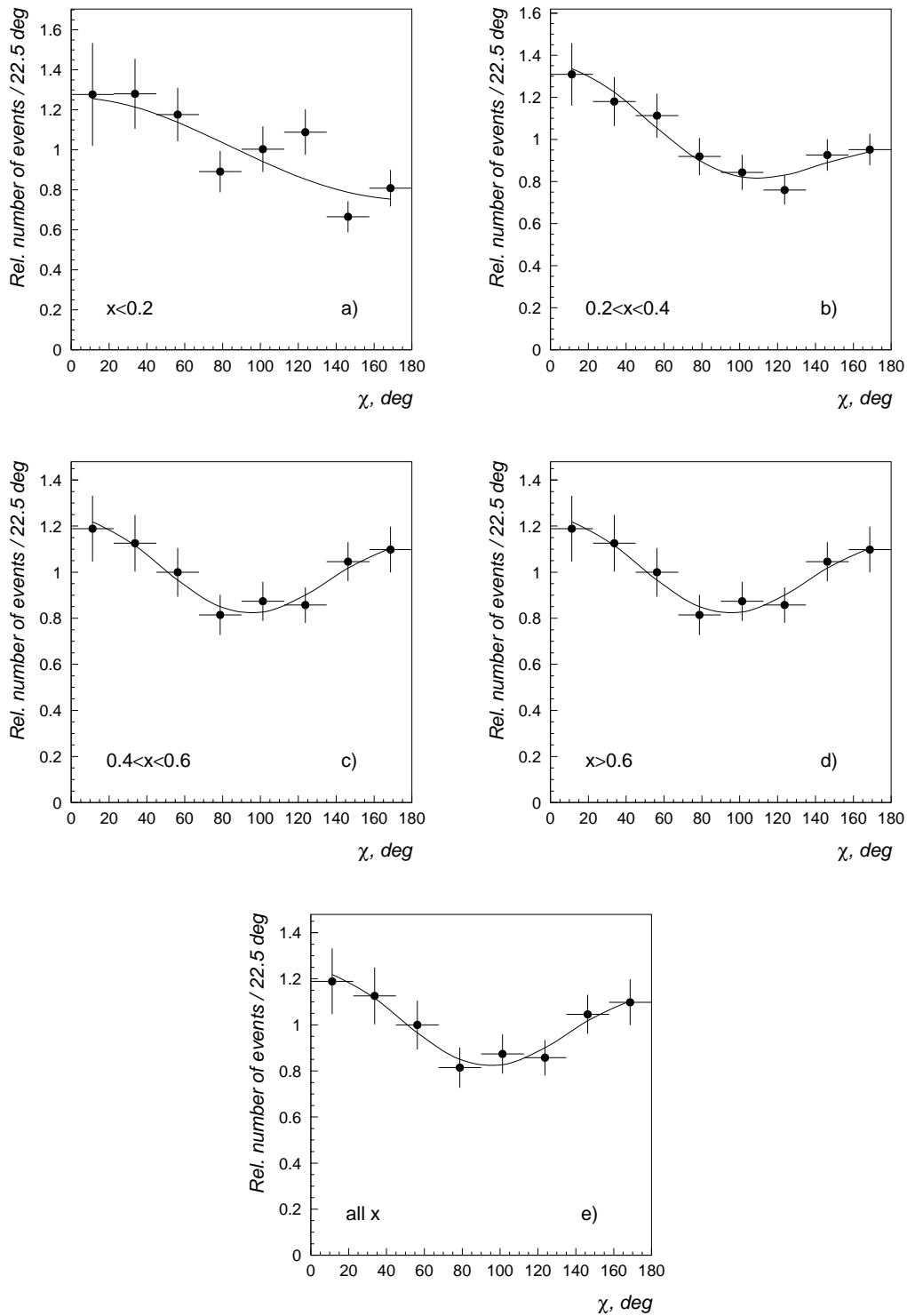
DELPHI

Figure 12: The same as Fig. 11 for the combined SAT and STIC samples.
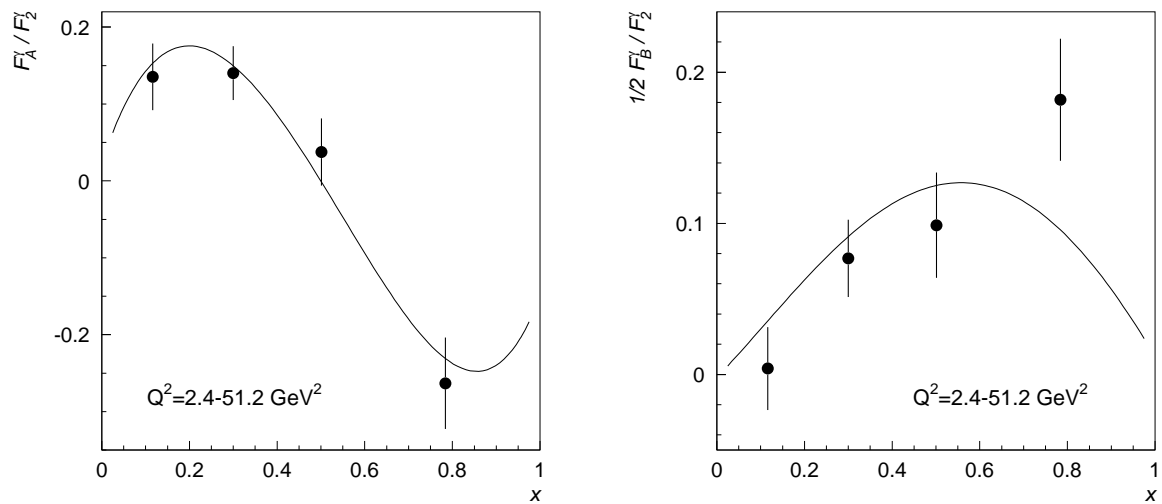
DELPHI

Figure 13: Ratios of leptonic structure functions F_A^γ/F_2^γ (left) and $\frac{1}{2}F_B^\gamma/F_2^\gamma$ (right) averaged in the Q^2 range from 2.4 to 51.2 GeV^2 as functions of x. The lines show the QED predictions from [18]. The points are plotted at the x values where the QED prediction is equal to its mean value over the x bin.